Available online at www.sciencedirect.com
SCIENCE DIRECT
Journal of Constructional Steel Research 62 (2006) 521–531
JOURNAL OF CONSTRUCTIONAL STEEL RESEARCH
www.elsevier.com/locate/jcsr

Dynamic buckling of anchored steel tanks subjected to horizontal earthquake excitation

J.C. Virella[a], L.A. Godoy[a,b,*], L.E. Suárez[a]

[a] *Department of Civil Engineering and Surveying, University of Puerto Rico, Mayagüez, 00681-9041, Puerto Rico*
[b] *Civil Infrastructure Research Center, Department of Civil Engineering and Surveying, University of Puerto Rico, Mayagüez, 00681-9041, Puerto Rico*

Received 20 July 2005; accepted 11 October 2005

Abstract

We investigate dynamic buckling of aboveground steel tanks with conical roofs and anchored to the foundation, subjected to horizontal components of real earthquake records. The study attempts to estimate the critical horizontal peak ground acceleration (Critical PGA), which induces elastic buckling at the top of the cylindrical shell, for the impulsive hydrodynamic response of the tank–liquid system. Finite elements models of three cone roof tanks with height to diameter ratios (H/D) of 0.40, 0.63 and 0.95 and with a liquid level of 90% of the height of the cylinder were used in this study. The tank models were subjected to accelerograms recorded during the 1986 El Salvador and 1966 Parkfield earthquakes, and dynamic buckling computations (including material and geometric non-linearity) were carried out using the finite element package ABAQUS. For the El Salvador accelerogram, the critical PGA for buckling at the top of the cylindrical shell decreased with the H/D ratio of the tank, while similar critical PGAs regardless of the H/D ratio were obtained for the tanks subjected to the Parkfield accelerogram. The elastic buckling at the top occurred as a critical state for the medium height and tallest models regardless of the accelerogram considered, because plasticity was reached for a PGA larger than the critical PGA. For the shortest model ($H/D = 0.40$), depending on the accelerogram considered, plasticity was reached at the shell before buckling at the top of the shell.

Keywords: Steel tanks; Stability; Buckling; Shells; Finite elements; Earthquake response

1. Introduction

Reports of damage to structures after major earthquakes provide evidence of failure and extensive damage in aboveground steel storage tanks. Cooper and Wachholz [1] reported damage of petroleum steel tanks due to the earthquakes of 1933 Long Beach, 1952 Kern County, 1964 Alaska, 1971 San Fernando, 1979 Imperial Valley, 1983 Coalinga, 1989 Loma Prieta, 1992 Landers, 1994 Northridge, and 1995 Kobe. Evidence of damage to petroleum steel tanks during recent earthquakes in India and Turkey was compiled by Jain et al. [2] and Suzuki [3]. A recently published report by an EERI reconnaissance team [4] describes the buckling of two aboveground steel storage tanks during the 2003 San Simeon earthquake in California.

The American Lifelines Alliance (ALA) [5] has collected different modes of failure that were observed in tanks during past earthquakes. These failure modes include shell buckling mode, roof damage, anchorage failure, tank support system failure, foundation failure, hydrodynamic pressure failure, connecting piping failure, and manhole failure. Among these different modes of failure, our main interest in this paper is the shell buckling mode.

The buckling behavior of steel tanks under seismic excitation identified by means of experimental and computational studies is usually classified as elasto-plastic buckling and elastic buckling. The elasto-plastic buckling behavior is associated with elephant foot buckling, which is characterized by an outward bulge just above the base of the tank [6]. Diamond shape buckling at the bottom of the tank has also been described as elastic buckling in Ref. [6]. Elastic buckling includes buckling at the top part of the cylindrical tank and shear buckling of the

* Corresponding author at: Department of Civil Engineering and Surveying, University of Puerto Rico, Mayagüez, 00681-9041, Puerto Rico. Tel.: +1787 265 3815; fax +1787 833 8260.
E-mail addresses: jvirella@uprm.edu (J.C. Virella), lgodoy@uprm.edu (L.A. Godoy), lsuarez@uprm.edu (L.E. Suárez).

0143-974X/$ - see front matter © 2005 Elsevier Ltd. All rights reserved.
doi:10.1016/j.jcsr.2005.10.001

shell. Shear buckling for tanks in the elastic range has been reported by Teng and Rotter [7].

Buckling modes with deflections at the top of the cylindrical part were described by Liu and Lam [8], Natsiavas and Babcock [9], Nagashima et al. [10], Redekop et al. [11] and Morita et al. [12]. The dynamic buckling studies by Natsiavas and Babcock [9] considered an open-top tank under horizontal harmonic base acceleration for a tall tank with a height to diameter ratio $H/D = 2.1$. Dynamic and static experimental studies were performed by Nagashima et al. [10] and Morita et al. [12] for tall tanks with a roof. Nagashima et al. [10] considered horizontal and vertical harmonic base acceleration for tanks with $H/D = 2$, while horizontal and vertical harmonic and simulated earthquake excitation were used by Morita et al. [12] for tanks in nuclear facilities with $H/D = 1.2$ and 1.3. The buckling at the top of a tank due to earthquakes has frequently been attributed to the sloshing component of the hydrodynamic response of the tank–liquid system [13]. However, both Morita et al. [12] and Natsiavas and Babcock [9] proved that this buckling mode arises mostly from the impulsive action of the hydrodynamic response of the liquid; the sloshing action may contribute to the occurrence of this type of buckling, but it is not the main cause.

Early investigations into the seismic behavior of anchored liquid storage tanks studied the effect of the hydrodynamic fluid–structure interaction on the seismic response. Housner [14], Haroun and Housner [15], Veletsos and Yang [16], and Veletsos [17] reported that a circular cylindrical tank containing liquid develops a cantilever-beam type mode when subjected to horizontal excitations. Housner [14] evaluated the hydrodynamic response for the tank–liquid system as the contribution of two different components: the impulsive liquid mode and the convective mode. The liquid in the upper portion of the tank vibrates with a long period sloshing motion, while the rest moves rigidly with the tank with an impulsive mode.

According to Housner [14], the impulsive and convective components should be separated to characterize the hydrodynamic response of tank–liquid systems excited horizontally, and this approach is adopted here. These two actions may be considered uncoupled in most cases, because there are significant differences in the natural periods of the impulsive and convective components of liquid motion [18], even though most of the response is effected by the motion of the liquid due to the impulsive component.

This study presents dynamic buckling analyses of anchored steel tanks subjected to horizontal earthquake excitations using three dimensional finite element models. Only the impulsive component of the hydrodynamic response of the tank–liquid systems is considered (the sloshing component is not included in the analyses). This paper concentrates on elastic buckling at the top of the cylindrical shell of broad tanks with geometries that are typical of petroleum tank farms, i.e. height to diameter ratios (H/D) below 1.0. The effect of the shell geometry, as reflected by the height to diameter ratio (H/D) and the slenderness ratio (D/t), is also studied.

2. Finite element model of the tank and the liquid

2.1. Tank models

To illustrate the nonlinear dynamic behavior of tanks, three geometric configurations are used in this paper (see Fig. 1), with height to diameter (H/D) ratios of 0.40 (Model A), 0.63 (Model B) and 0.95 (Model C). Experience from past earthquakes has shown that tanks that are completely filled with liquid are more prone to suffer damage [5], thus this study considers a liquid level of 90% of the height of the tank with a 10% freeboard. The tapered thicknesses for the tanks considered were designed for this study using the API 650 provisions for serviceability conditions [19]. No seismic design considerations were taken into account. The tanks are modeled with a cone roof supported by roof rafters.

The finite element meshes of the three dimensional tank models use shell elements for the cylinder and the roof, and beam elements for the roof rafters. The tank bottom was not modeled, since only anchored tanks are considered, and our primary interest is in the buckling of the cylinder shell. All models have clamped condition at the base.

The finite element analysis package ABAQUS [20] was used to carry out all computations, using its quadrilateral shell elements S4R for the cylinder, triangular shell elements S3R for the roof, and beam elements B31 for the roof rafters. The S4R is a four-node, doubly curved shell element with reduced integration, hourglass control, and finite membrane strain formulation. The S3R element is a three node degenerated version of the S4R with finite membrane strain formulation. The B31 is a two node linear beam element in space. The characteristics of these elements are described in ABAQUS [21]. Finite element meshes of 9262 elements for Model A and 10 942 elements for Models B and C were employed to assure convergence of the solution.

2.2. Tank–liquid models

The liquid is modeled using an added mass approach, in which the mass is obtained from a pressure distribution for the impulsive mode of a tank–liquid system originally developed by Veletsos and Shivakumar [22]. This pressure distribution is due to the rigid body horizontal motion of a rigid tank–liquid system, and is described as

$$P_i(\eta, \theta, t) = c_i(\eta)\, \rho R \ddot{x}_g(t) \cos\theta \tag{1}$$

where P_i is the impulsive pressure; η is a non-dimensional vertical coordinate $= z/H_L$; z is the vertical coordinate measured from the tank bottom; R is the tank radius; $\ddot{x}_g(t)$ is the ground acceleration; and t is the time. The function $c_i(\eta)$ defines the impulsive pressure distribution along the cylinder height, and is computed as

$$c_i(\eta) = 1 - \sum_{n=1}^{\infty} c_{cn}(\eta) \tag{2}$$

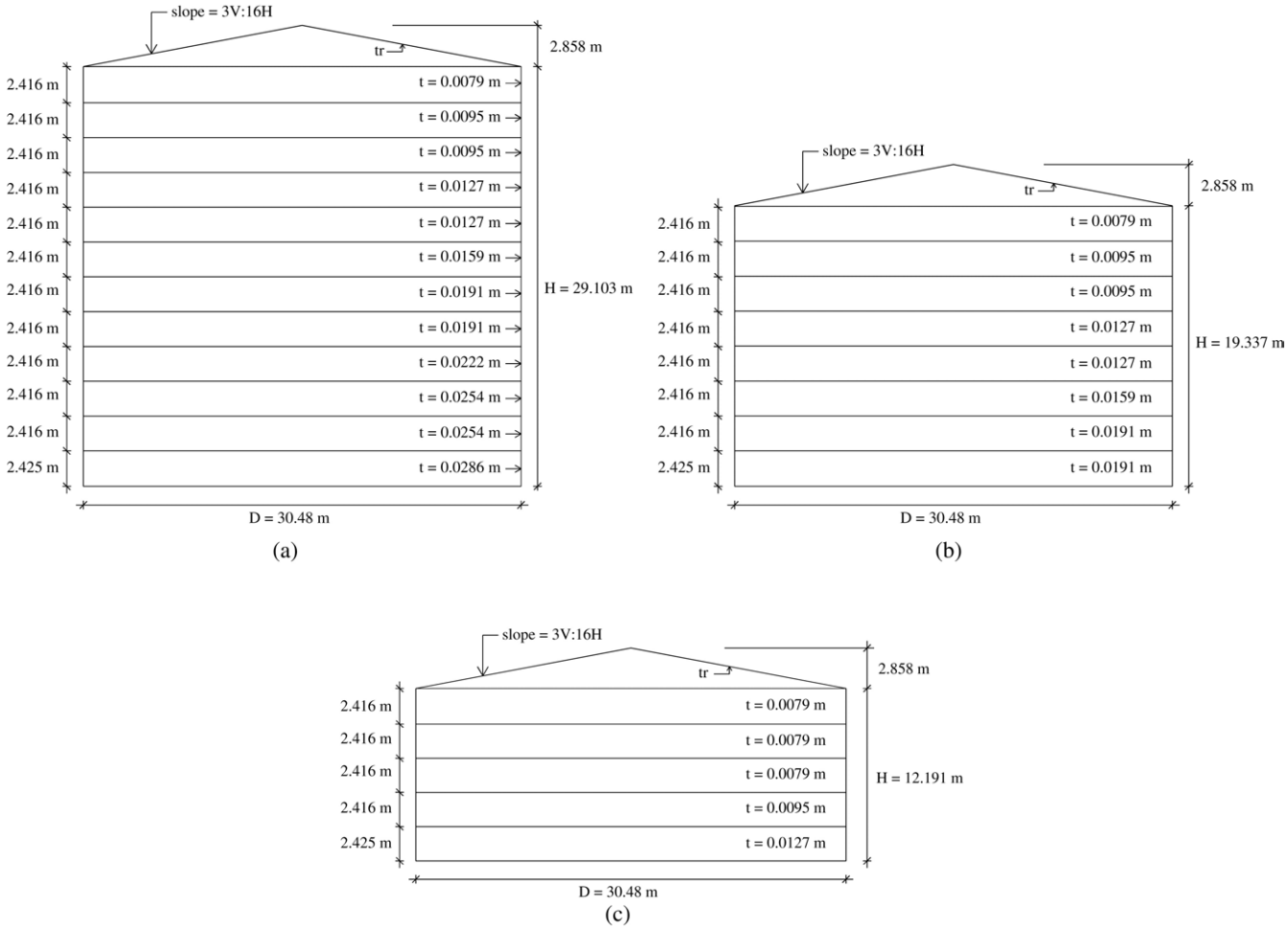

Fig. 1. Tank models with cone roof supported by rafters; t = shell thickness, tr = roof thickness; tr = 6.35 mm (roof with rafters): (a) tank with $H/D = 0.95$; (b) tank with $H/D = 0.63$; (c) tank with $H/D = 0.40$.

where $c_{cn}(\eta)$ is a function that defines the convective pressure distribution along the cylinder height, and takes the form

$$c_{cn}(\eta) = \frac{2}{\lambda_n^2 - 1} \frac{\cosh[\lambda_n (H/R)\eta]}{\cosh[\lambda_n (H/R)]}. \quad (3)$$

The parameter λ_n is the nth root of the first derivative of the Bessel function of the first kind and first order. The first three roots are $\lambda_1 = 1.841$, $\lambda_2 = 5.311$, and $\lambda_3 = 8.536$. The function $c_i(\eta)$ converges rapidly with the number of terms in the summation in Eq. (2), and thus it is sufficient to include three coefficients c_{cn}. The pressure distributions defined in Eq. (1) for each of the tank–liquid systems considered in this paper and for $\theta = 0$ are presented in Fig. 2. The procedure used to obtain the added mass from the pressure distribution from Eq. (1) was presented by Virella [23]. The ratios of the total impulsive mass to the total mass of the liquid were computed for all the tank–liquid systems, and there are only 5% differences to those recommended by Housner [14].

The added liquid mass in lumped form was attached to the shell nodes by means of massless spring elements considered as rigid links, as shown in Fig. 3. The one-direction springs had supports oriented in their local axes that constrained the motion of the nodal masses to the normal direction of the shell. The motions of each support are restricted in the global tangential direction (i.e. perpendicular to the element axis) and in the vertical direction, whereas it is free to move in the radial direction (i.e. local axial direction of the spring). The sum of the total liquid nodal masses in a specific direction is twice that computed by using the expression due to Housner [14]. However, as the liquid masses can only move in the radial

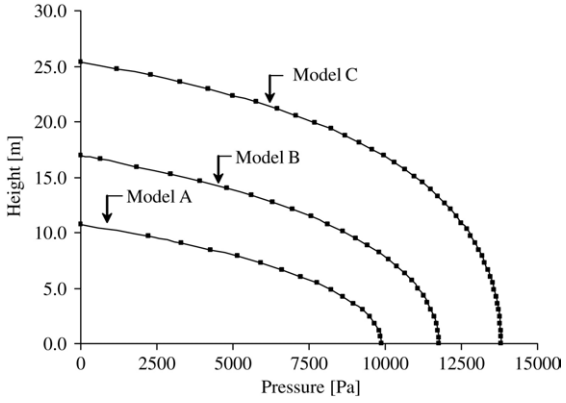

Fig. 2. Impulsive pressure for the tank–liquid systems with $\ddot{x}_g = 1$ m/s^2: (a) $H/D = 0.40$; (b) $H/D = 0.63$; (c) $H/D = 0.95$.

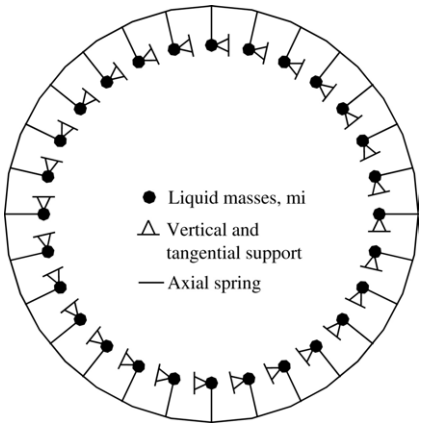

Fig. 3. Model with normal mass around the circumference.

direction, then only half of this total impulsive mass is excited in a specific direction.

3. Dynamic buckling estimates

Geometric and material non-linearity was considered in the dynamic buckling analyses of the tank–liquid systems. The excitation was introduced in terms of the impulsive pressure presented in Eq. (1), with a time variation equal to the horizontal base acceleration induced by the earthquake.

The load factor λ assumed for the dynamic buckling analyses is the horizontal peak ground acceleration (PGA) of an earthquake. The impulsive pressures were normalized with respect to the acceleration of gravity ($1g$), so that the critical load factor provides the PGA that produces buckling of the shell. The load factor λ is the maximum amplitude of the time variation of the impulsive pressures. This load factor was increased successively for each analysis until buckling was detected.

An initial analysis step is performed, loading the tank with the hydrostatic pressure and the self-weight. This step is solved in ABAQUS [20] by means of a quasistatic dynamic analysis and by including geometric non-linearity so that the stiffness matrix of the system is modified by the presence of the initial loads. The dynamic buckling analyses are carried out in a second step. The non-linear equation of motion solved in the dynamic buckling analyses has the form

$$[M]\{\ddot{u}(t)\} + [C]\{\dot{u}(t)\} + [K_T]\{u(t)\} = -F(t) \quad (4)$$

$$F(t) = [M_s]\{r_x\}\ddot{x}_g(t) + \{P_i\}\,\ddot{x}_g\,(t) \quad (5)$$

$$\ddot{x}_g\,(t) = \mathrm{PGA} * f\,(t) \quad (6)$$

where $[M]$, $[C]$ and $[K_T]$ are, respectively, the mass, damping and stiffness matrices of the tank–liquid system considering material and geometric non-linearity, $\{u(t)\}$, $\{\dot{u}(t)\}$ and $\{\ddot{u}(t)\}$ are, respectively, the displacement, velocity and acceleration vectors, $\{r_x\}$ is the vector of influence coefficients containing ones at the degrees of freedom in the direction of the applied earthquake, $\ddot{x}_g(t)$ is the horizontal acceleration record, $\{P_i\}$ is the vector of nodal forces computed from the impulsive hydrodynamic pressures normalized for an acceleration of $1g$, $[M_s]$ is the mass matrix of the shell, and $f\,(t)$ is the time variation of the earthquake accelerogram.

Table 1
Mass proportional damping coefficients for tank models

Model	T_{fund}	ζ (%)	α
A	0.21	2.0	1.20
B	0.24	2.0	1.05
C	0.30	2.0	0.84

T_{fund} = period of fundamental mode; ζ = modal damping ratio; α = mass proportional damping coefficient.

The procedure for obtaining the dynamic buckling loads can be divided into three steps. First, the model of the tank–liquid system is defined; second, an earthquake accelerogram is selected in order to perform the dynamic buckling simulations; and third, dynamic buckling is identified by means of a buckling criterion.

3.1. Models used for the tank–liquid systems

The model of the tank–liquid system used for the dynamic buckling analyses required us to consider many aspects, which are described next. First, the methodology described in the previous section was used to establish the impulsive pressure and aggregated mass of the tank–liquid system. Second, viscous damping was introduced in the model by means of a Rayleigh mass proportional damping. The damping coefficient selected was based on the natural frequency of the fundamental mode of each tank–liquid system, which was obtained in a previous study [24]. The damping coefficients and the fundamental periods for all the tank–liquid systems considered are presented in Table 1. Third, the plasticity of the shell was modeled using the von Mises yield criterion, an elasto-plastic model, and a yield stress (steel) of 248 MPa. Fourth, an explicit time integration technique available in ABAQUS [20] was used to solve the dynamic analysis of the tank–liquid systems. In this way, the duration of the simulation was significantly reduced compared to solutions which use direct integration procedures. Many analyses runs were required to obtain the dynamic buckling load (λ_{crit}) for each tank–liquid system, so that reducing the computer time of the simulation was an essential part of the dynamic buckling analyses.

3.2. Selection of the earthquake accelerogram

Design codes such as the 1997 UBC [25] recommend using at least three earthquake accelerograms for time history analyses. Because they will have significant amplitudes over a wide range of input frequencies, this would require extensive computer time in the present case. For example, four seconds of input motion takes an average of about 10 h with a 3.0 GHz Pentium processor. Therefore, only two accelerograms were used for the numerical computations.

Accelerograms with dominant frequencies of about 1–10 Hz were selected, since typical earthquake records have dominant frequencies in that range [26]. Accelerograms with strong motion durations larger than about 10 s were discarded, and

attention was then directed toward accelerograms from near earthquakes, recorded in rock, with small duration.

The east–west component of an accelerogram recorded at the Geotechnical Investigation Center (CIG) during the El Salvador earthquake of October 10, 1986 (Fig. 4(a)) was selected for the analyses. This earthquake had a moment magnitude of 5.6, and the accelerogram was characterized by PGA = 0.69g, with an epicentral distance of 4.3 km, a focal depth of 7.3 km, and a total duration of 9.04 s. This accelerogram was recorded very close to the earthquake source. The fact that the earthquake source was very shallow led to the short duration (9.04 s). The earthquake record is adequate for dynamic buckling analyses because it has short duration, with the maximum amplitudes occurring during the first four seconds. It was decided to perform the computations using a portion of the earthquake record, with sufficient time (3.98 s) to capture the frequency content of the original accelerogram. The maximum amplitudes of the earthquake occur before the first four seconds of motion (see Fig. 4(a)). The acceleration is close to zero at that time and the frequency content of the original record and the shortened record are similar, as can be seen from Fig. 4(b) and (c).

An accelerogram from the 1966 Parkfield earthquake, presented in Fig. 5, was also chosen for the same reasons as discussed previously. This is an accelerogram recorded in rock, with a magnitude of 5.5, a focal depth of 6 km, and an epicentral distance of 27 km. An excitation duration of 7 s was considered for the numerical computations.

3.3. Dynamic buckling criteria

The Budiansky and Roth [27] criterion, which has been used extensively in the literature to determine the dynamic buckling load of structures, is employed in this paper. According to this criterion, different analyses of the structure for several load levels need to be done, and the value for which there is a significant jump in the response for a small increase in the load indicates that the structure passes from a stable state to a critical state. For seismic stability analyses, there is a problem with this criterion due to the cyclic nature of the earthquake loading. As the direction of loading is not maintained for long enough to produce a very high jump in the displacements without loading in the opposite direction, it is sometimes difficult to identify the occurrence of buckling.

Babcock et al. [28] performed experiments on the dynamic buckling of a nuclear steel containment subjected to a horizontal base motion applied in a single axis, and used the Budiansky–Roth criterion to identify the dynamic buckling state of the system by measuring the shell displacements. Tanami et al. [29] studied the dynamic buckling of a reticulated single-layer dome considering a step load to represent the up and down earthquake excitation, and used the Budiansky–Roth and the Fourier spectrum criteria. They monitored the load level that generated a suddenly large displacement, and also observed the change in the predominant frequencies of the system, as a node response passed from a pre-buckling to a buckled load level. Other studies, such as Auli and Rammerstorfer [30] and Hjelmstad and Williamson [31], used a phase plane criterion.

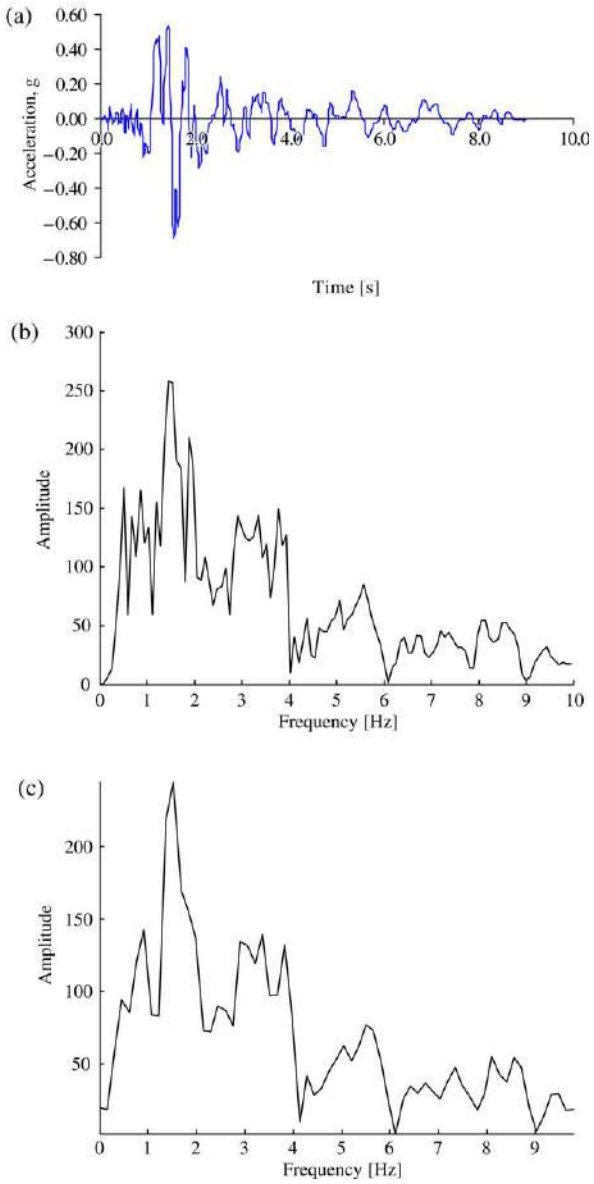

Fig. 4. The 1986 El Salvador earthquake record; PGA = 0.69g. (a) East–west component of an accelerogram recorded at the Center of Geotechnical Investigations (CIG). (b) Fourier amplitude spectrum for the total duration of the accelerogram. (c) Fourier amplitude spectrum for the accelerogram with reduced duration.

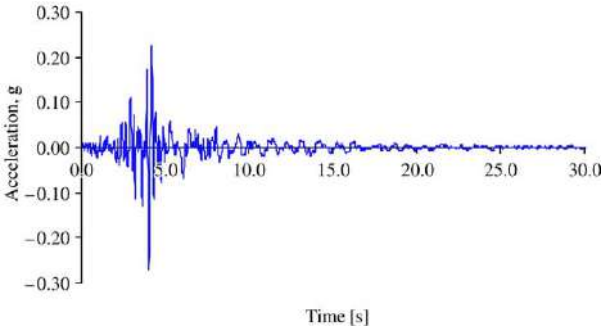

Fig. 5. Accelerogram recorded during the Parkfield (1966) earthquake, in California; PGA = 0.27g. Reference: NOAA, Usaca 01.109.

4. Dynamic buckling results

Dynamic buckling analyses of tank–liquid systems were performed using the accelerograms from the 1986 El Salvador and 1966 Parkfield earthquakes. Plasticity was included in the analyses to identify whether the buckling at the top of the cylindrical shell of the tank occurs before or after yielding.

Two types of seismic behavior for the tank–liquid systems subjected to horizontal seismic excitations were found in this study. In the first case, elastic buckling was observed to initiate at the top part of the cylindrical shell prior to the occurrence of plasticity. In the second case, buckling occurred at the top of the cylindrical shell after material plasticity was observed at the mid-part of the shell.

Depending on the tank height, two different dynamic buckling responses were observed for the tank–liquid systems subjected to the earthquake excitations. For Models B ($H/D = 0.63$) and C ($H/D = 0.95$) a jump in the displacements was clearly observed in the equilibrium response for a small increase in the amplitude of the excitation, from which the critical state could be clearly identified. For Model A ($H/D = 0.40$), the displacements at the cylinder increased successively with the load, with no clear jump in the displacements. Both buckling cases were characterized by elastic buckling, as plasticity at the region where buckling took place was never reached before the first instability occurred.

4.1. Model A ($H/D = 0.40$)

Fig. 6 shows the plots used to determine dynamic buckling, for tank Model A subjected to the 1986 El Salvador accelerogram. This figure displays the transient response for different levels of excitation in which a jump in the displacement field can be observed for PGAs above $0.35g$. The peaks in the transient response are studied in detail in Fig. 7 by plotting the PGA versus the maximum radial displacement at the node considered. This is not an equilibrium path in the sense of static stability [32], but it is a useful plot to identify the nature of the nonlinear dynamic response as it evolves for different PGA levels. Such plots were originally employed by Budiansky and Roth [27]. In this paper, we shall refer to them as "pseudo equilibrium paths".

A similar behavior was obtained for the tank Model A subjected to the 1966 Parkfield accelerogram, as is also illustrated in Fig. 7. The pseudo equilibrium paths in Fig. 7 show the systems approaching a maximum PGA, as the stiffness is progressively reduced. Two different responses can be identified from the pseudo equilibrium paths. At small displacements, the curve follows an initially stable path, with the slope corresponding to the initial stiffness of the system. A second trend can be observed for higher PGA, associated with a reduction in the stiffness. The pseudo equilibrium path was then approximated by a bilinear trace, as shown in Fig. 7, and the intersection of the two lines indicate the critical PGA, i.e. the excitation level at the transition from the initially stable to an unstable path. The linear regressions used for the bilinear models produced a good fit, as the coefficient of determination

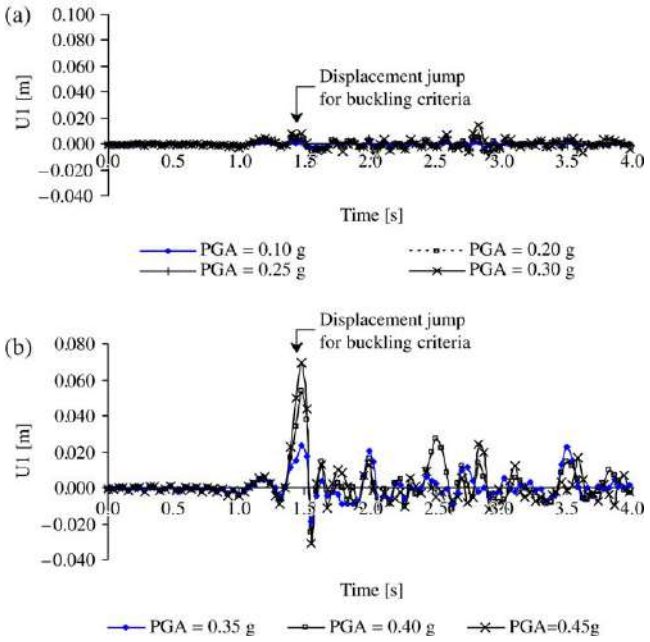

Fig. 6. Transient response for Model A, subjected to the 1986 El Salvador accelerogram. (a) PGA = $0.10g$–$0.30g$; (b) PGA = $0.35g$–$0.45g$.

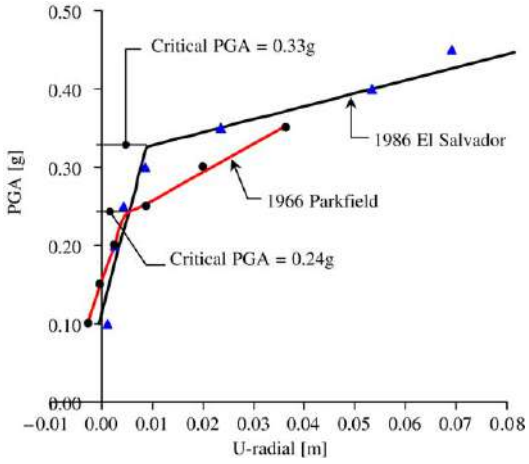

Fig. 7. Pseudo equilibrium paths for critical node (node A, see Fig. 18) at the buckling zone of Model A.

of the regression was in all cases close to 1.0. A buckling mode with large deflections at the top occurred in both cases, and a smaller critical PGA was found for Model A using, as seismic demand, the 1966 Parkfield accelerogram (Critical PGA = $0.24g$) compared with that using the 1986 El Salvador accelerogram (Critical PGA = $0.33g$).

For the 1986 El Salvador accelerogram, plasticity occurred in Model A for a PGA = $0.35g$ (see Fig. 8), which is a larger value than that required for the elastic buckling mode. Therefore, elastic buckling at the top of the shell occurred as a critical state, before plasticity was reached at any part of the shell. For the 1966 Parkfield accelerogram, plasticity was reached at the middle of the tank at a PGA = $0.20g$ (see Fig. 10), which is smaller than the PGA obtained for the elastic buckling at the top of the shell (PGA = $0.24g$, see Fig. 9).

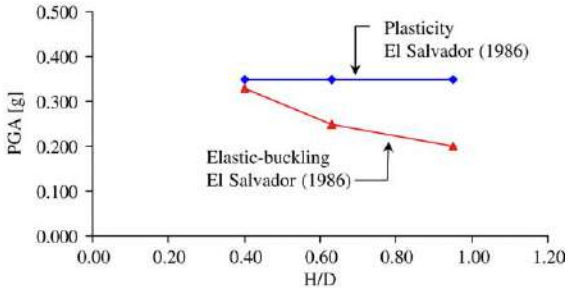

Fig. 8. Peak ground accelerations for elastic buckling modes and plasticity for the three tank models for the 1986 El Salvador accelerogram.

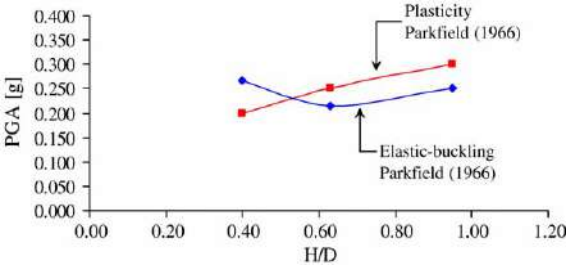

Fig. 9. Peak ground accelerations for elastic buckling modes and plasticity for the three tank models for the 1966 Parkfield accelerogram.

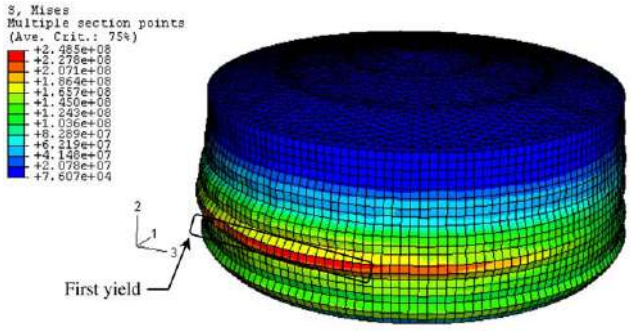

Fig. 10. Von Mises stresses for Model A subjected to the 1966 Parkfield accelerogram with PGA = 0.20g, showing that first yield occurs at the bottom of the shell.

4.2. *Models B* ($H/D = 0.63$) *and C* ($H/D = 0.95$)

The transient response leading to dynamic buckling of tank Model C subjected to the 1986 El Salvador accelerogram is shown in Fig. 11 for several levels of horizontal PGA. The first jumps in the transient response, for which the pseudo equilibrium path in Fig. 12 was constructed, are indicated in Fig. 11.

For a 20% change in PGA (from 0.20g to 0.25g) the pseudo equilibrium path shows that the radial displacements increase by 170% (from 0.019 m to 0.0522 m), so that the first instability for Model C occurs for a PGA of about 0.20g.

A similar behavior was obtained for tank Model C subjected to the 1966 Parkfield accelerogram, and for Model B subjected to both the 1986 El Salvador and 1966 Parkfield records, which buckled with a jump in the displacements. The pseudo equilibrium path for Model B subjected to the 1986 El Salvador accelerogram is presented in Fig. 12, in which a critical PGA of 0.25g is identified.

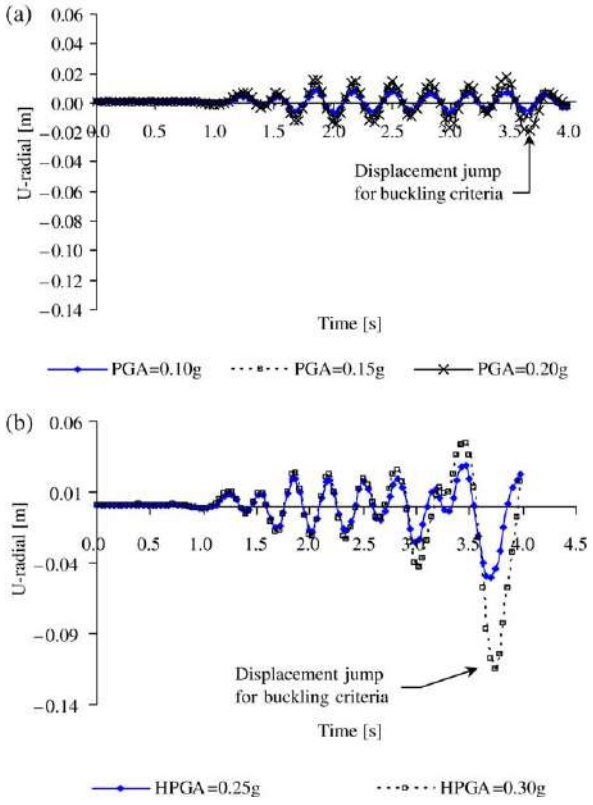

Fig. 11. Transient responses for critical node (node A, see Fig. 19) at buckling zone of Model C, subjected to the 1986 El Salvador accelerogram: (a) PGA = 0.10g–0.20g; (b) PGA = 0.25g–0.30g.

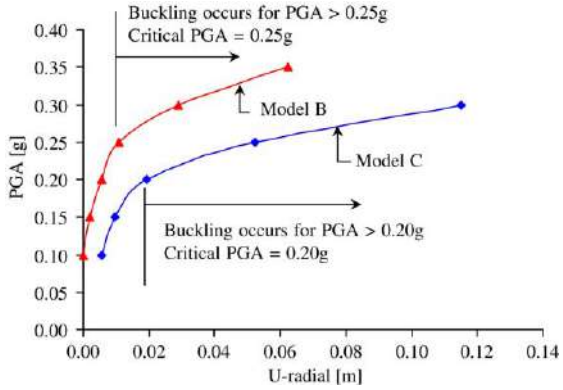

Fig. 12. Pseudo equilibrium paths for critical node (node A, see Fig. 19) at the buckling zone of Models B and C subjected to the 1986 El Salvador accelerogram.

Plasticity was first reached for Models B and C at mid-height or at the bottom of the shell (see Fig. 13) for PGAs larger than that found for the elastic buckling at the top of the cylindrical shell, as illustrated in Figs. 8 and 9. Therefore, for Models B and C, elastic buckling at the top of the cylindrical shell occurred before plasticity was reached at any part of the shell.

4.3. *Comparisons on dynamic buckling characterization*

The critical PGAs for the dynamic buckling mode corresponding to elastic buckling with a deflected shape at the top of the cylindrical shell are summarized in Fig. 14. The three

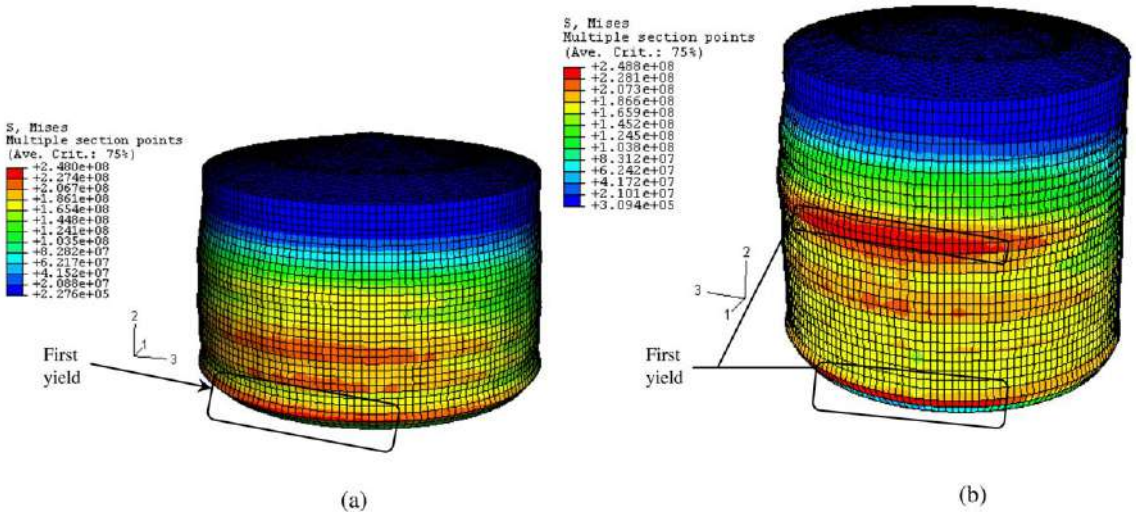

Fig. 13. Von Mises stresses for tanks subjected to the 1986 El Salvador accelerogram with PGA = 0.35g, showing the first yield at loads higher than elastic buckling (Critical PGA). (a) Model B. (b) Model C.

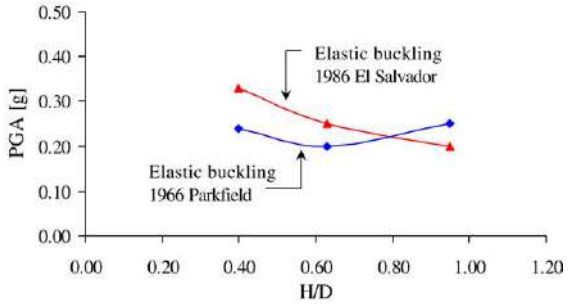

Fig. 14. Variation of the critical PGA with H/D for the elastic buckling mode.

tank–liquid systems were subjected to the 1986 El Salvador and 1966 Parkfield accelerograms. For the tanks subjected to the 1986 El Salvador accelerogram, the critical PGA decreases with an increase in H/D, so that the lowest critical PGA was obtained for $H/D = 0.95$ (Model C), and the highest for $H/D = 0.40$ (Model A). For the 1966 Parkfield accelerogram, similar critical PGAs were obtained regardless of the H/D of the tank model. However, a slightly smaller value was obtained for $H/D = 0.63$ (Model B).

In the theory of static elastic instability, buckling can occur in the form of a limit point or bifurcations. A structure that fails by limit point displays the same deflected shape even after buckling occurs, and there is an increase in the amplitude of the displacements until a maximum load is reached. An analogy can be established in this problem for Model A subjected to the 1986 El Salvador, in which the deflected shapes for a PGA below and above the critical PGA of 0.33g (at the same response time) are almost the same, as illustrated in Fig. 15. Ovaling vibration is observed at the top of the tank for the deformed shapes in the figure, i.e. both deformed shapes are similar and the differences affect just the amplitude of the displacements. By analogy, we shall refer to such behavior as a limit point in dynamic buckling.

However, this class of behavior was not uniform for all the cases investigated in this paper. For example, the deflected shapes for tank Model C for the El Salvador earthquake (Fig. 16) show a change in the pattern of displacements, and this is typical of what is known as a bifurcation in the theory of static buckling. By analogy, we shall refer to such behavior as bifurcation behavior in dynamic buckling.

4.4. Characterization of the buckling at the top of the cylinder

It is important to discuss the actual mechanism of dynamic buckling for the tank–liquid systems considered in this paper. Natsiavas and Babcock [9] have shown that the dynamic pressure in the fluid may induce a negative resultant pressure in the tank close to the free surface of the fluid, where the hydrostatic pressure is small. This negative resultant pressure ($P_{hyd} - P_{imp}$, in Fig. 17) can lead to local buckling of the tank, as illustrated in Fig. 17. Such negative pressures induce local compressive hoop stresses that may lead to local buckling of the tank.

The elastic buckling modes for the tanks considered in this study affect the top of the tank along the main direction of the excitation (i.e. for $\theta = 0$ in Eq. (1)), where the impulsive component of the hydrodynamic pressures have their maximum values and the shell thicknesses are smallest (see Fig. 1). This buckling was produced by the negative (inward) resultant pressure ($P_{hyd} - P_{imp}$, in Fig. 17) near the free surface of the fluid, which induced large compressive stresses sufficient to buckle the shell (see Fig. 17). Fig. 18 presents the hoop, vertical and shear maximum stresses for a critical element at the buckling zone of tank Model A ($H/D = 0.40$). This figure shows that the circumferential compressive membrane stresses are much larger than the vertical membrane stresses and shear stresses in the buckling region and thus are responsible for inducing local buckling in the tank shell. The maximum von Mises stresses in the buckling zone are about 88 MPa (35% of the yield stress, see Fig. 19), so that the steel remains elastic at the onset of dynamic buckling. A similar behavior was obtained for the other tank–liquid systems, as shown in Table 2.

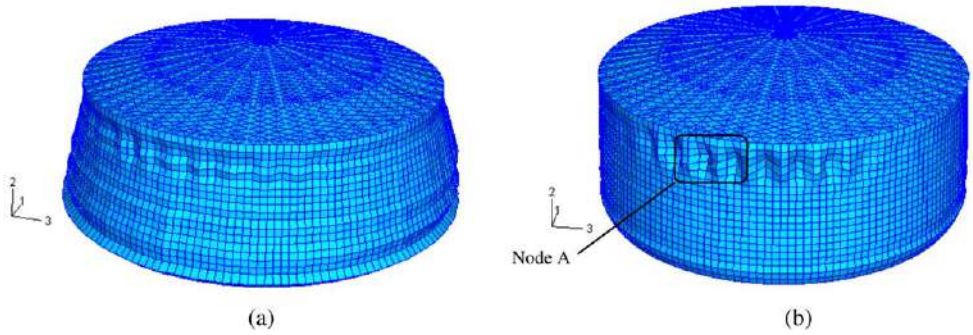

Fig. 15. Deformed shapes for tank Model A subjected to the 1986 El Salvador accelerogram, showing that the deflected mode is basically the same before and after the critical PGA: (a) PGA $= 0.25g$; (b) PGA $= 0.35g$.

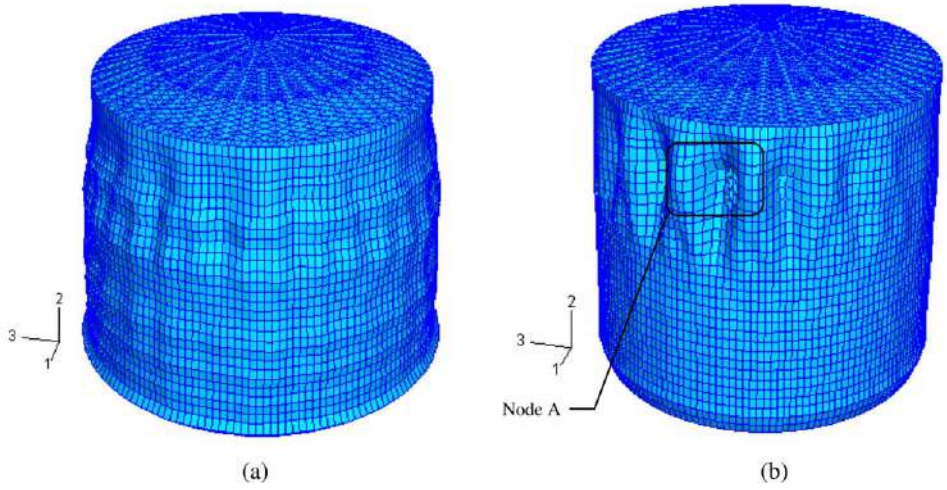

Fig. 16. Deformed shapes for tank Model C subjected to the 1986 El Salvador accelerogram, showing different deflected modes before and after the critical PGA: (a) PGA $= 0.15g$; (b) PGA $= 0.25g$.

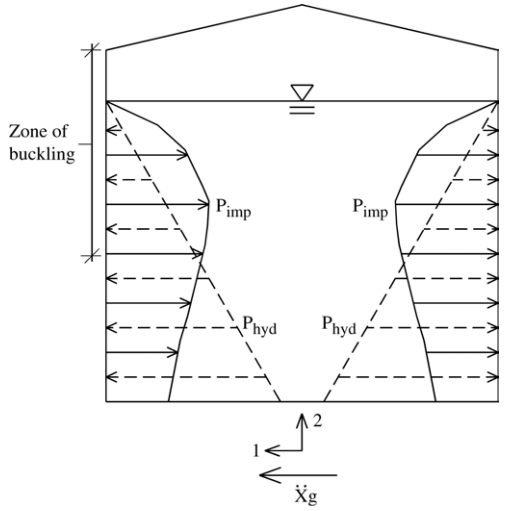

Fig. 17. Illustration of the buckling zone at the tank shell: P_{imp}= impulsive pressure; P_{hyd}= hydrostatic pressure; $\ddot{X}_g$= base acceleration.

5. Conclusions

Elastic dynamic buckling states for tank–liquid systems under horizontal earthquake excitation in which the buckling mode has deflections at the top of the cylindrical part of the shell have been obtained in this paper. Critical values of PGA for tanks filled with liquid up to 90% of the cylinder height are in the range between $0.25g$ and $0.35g$, so that this mode of failure should be of great concern to the designer. These levels of PGA are typical of those expected on favorable rock conditions on seismic zones 2 to 3 (out of 4 in the 1997 UBC scale, for instance) which are regions of moderate to not very high seismic activity. The geometry of the tank, as reflected by the aspect ratio H/D, has some influence on the critical PGA, but no clear trend was observed for all the earthquakes considered. For the 1986 El Salvador accelerogram, the critical PGA decreased with the H/D ratio of the tank, while similar PGAs were obtained for the 1966 Parkfield accelerogram regardless of the H/D ratio.

For the shortest ($H/D = 0.40$) and medium height ($H/D = 0.63$) tank models, the 1966 Parkfield earthquake was more critical than the 1986 El Salvador earthquake record; however, for the tallest tank ($H/D = 0.95$) the opposite occurred.

For the medium height ($H/D = 0.63$) and tallest tank ($H/D = 0.95$) models, elastic buckling at the top of the cylindrical shell occurred before plasticity. Only for the shortest model ($H/D = 0.40$) subjected to the 1966 Parkfield earthquake record, buckling at the top part of the cylindrical shell occurred after material plasticity. Here plasticity at the

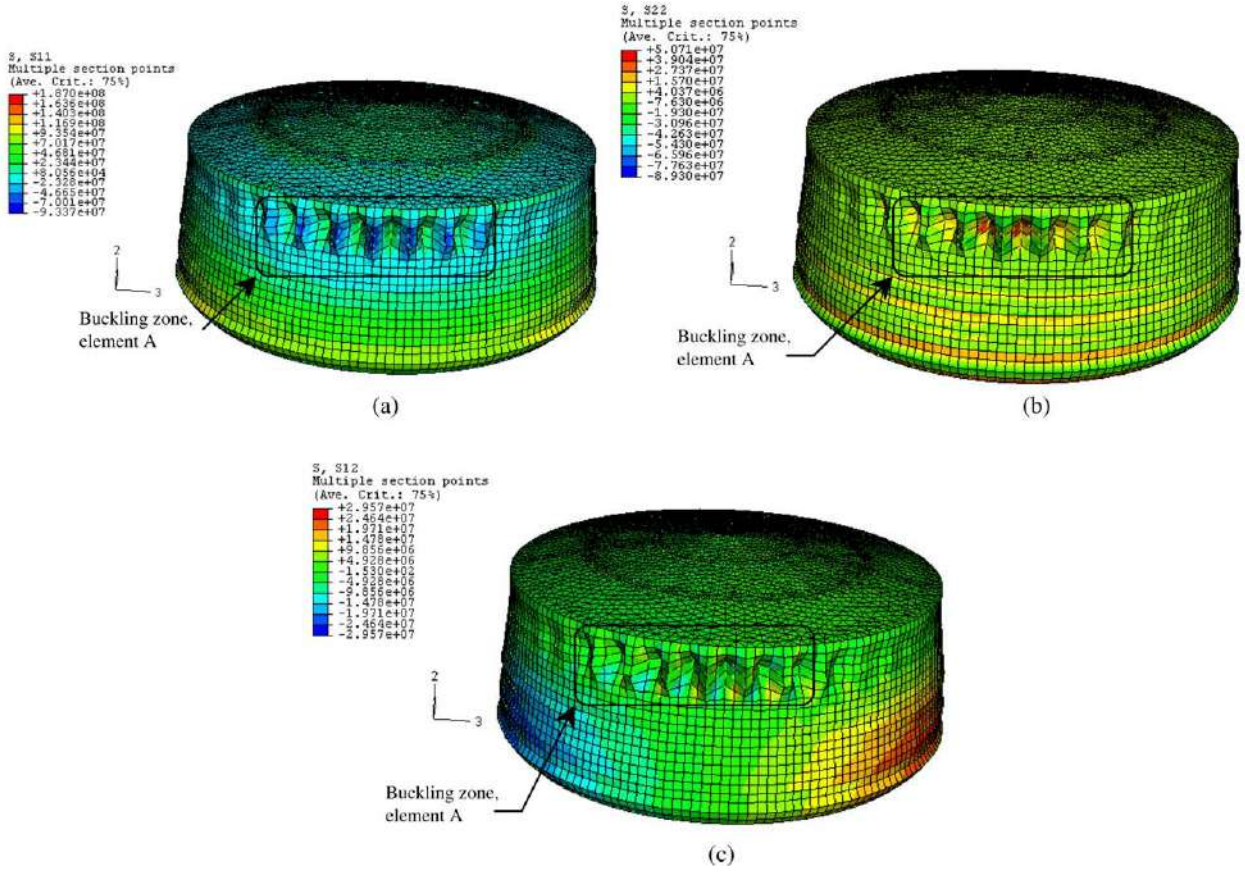

Fig. 18. Model A stresses for the displacement jump indicated in Fig. 7(b) and a PGA = 0.35*g*: (a) hoop stresses; (b) vertical stresses; (c) shear stresses.

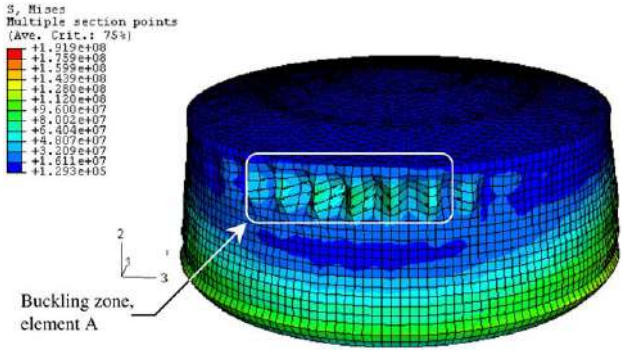

Fig. 19. Model A von Mises stresses for the displacement jump indicated in Fig. 7(b) and a PGA = 0.35*g*.

Table 2
Stresses for a critical element in the buckling zone (element A, Fig. 19) of Model A, under the 1986 El Salvador accelerogram

Model	H/D	PGA	Circumferential stresses (MPa)	Vertical stresses (MPa)	Shear stresses (MPa)
A	0.4	0.35	91.1 (C)	11.7 (C)	10.2
B	0.63	0.3	95.6 (C)	1.0 (T)	18.6
C	0.95	0.25	70.8 (C)	49.7 (C)	2.4

(C) = compressive stresses; (T) = tensile stresses.

tank mid-height occurred for a PGA smaller than that required for elastic buckling.

It is concluded that buckling at the top of the shell is caused by a negative (inward) net pressure at the zone in the tank where the impulsive hydrodynamic pressure induced by the earthquake excitation exceeds the hydrostatic pressure. This negative net pressure induces membrane compressive circumferential stresses which buckled the shell.

This agrees with previous observations made by Natsiavas and Babcock [9] on the subject.

Acknowledgements

J.C. Virella was supported by a PR-EPSCOR post-doctoral fellowship grant EPS-0223152 for this research. Partial support from the Mid-America Earthquake Center is also acknowledged.

References

[1] Cooper TW, Wachholz TP. Optimizing post-earthquake lifeline system reliability. In: Proceedings of the 5th US conference on lifeline earthquake engineering. ASCE, vol. 16. 1999. p. 878–86.
[2] Jain SK, Lettis WR, Murty CVR, Bardet J. Bjuh, India earthquake of January 26, 2001, reconnaissance report. Earthquake spectra (EERI) 2002; 8(Suppl. A): 257–95.
[3] Suzuki K. Report on damage to industrial facilities in the 1999 Kocaeli earthquake, Turkey. Journal of Earthquake Engineering 2002; 6(2):275–96.

[4] EERI Reconnaisance Team. The San Simeon, California, earthquake, December 22, 2003. EERI Learning from earthquakes reconnaissance report. 2005. p. 23–44.
[5] American Lifelines Alliance. Seismic fragility formulations for water systems. ASCE 2001. Part1-Guideline, Part-2 Appendices.
[6] Handam FH. Seismic behavior of cylindrical steel storage tanks. Journal of Construction Steel Research 2000;53:307–33.
[7] Teng JG, Rotter JM. Buckling of thin metal shells. London: Spon Press, Taylor and Francis; 2004.
[8] Liu WK, Lam D. Nonlinear analysis of liquid filled tank. ASCE Journal of Engineering Mechanics 1983;109(6):1344–57.
[9] Natsiavas S, Babcock CD. Buckling at the top of a fluid-filled tank during base excitation. ASME Journal of Pressure Vessel Technology 1987;109: 374–80.
[10] Nagashima H, Kokubo K, Takayanagi M, Saitoh K, Imaoka T. Experimental study on the dynamic buckling of cylindrical tanks [Comparison between static buckling and dynamic buckling]. JSME International Journal 1987;30(263):737–46.
[11] Redekop D, Mirfakhraei P, Muhammad T. Nonlinear analysis of anchored tanks subject to equivalent seismic loading, In: Proceedings of the ASME pressure vessels and piping conference, vol. 442. 2002. p. 157–63.
[12] Morita H, Ito T, Hamada K, Sugiyama A, Kawamoto Y, Ogo H et al. Investigation on buckling behavior of liquid storage tanks under seismic excitation: 2nd report – Investigation on the nonlinear ovaling vibration at the upper wall. Proceedings of the ASME pressure vessels and piping conference, vol. 466. 2003. p. 227–34.
[13] Malhotra PK. Practical nonlinear seismic analysis of tanks. Earthquake Spectra 2000;16(2):473–92.
[14] Housner GW. The dynamic behavior of water tanks. Bulletin of the Seismological Society of America 1963;53(2):381–9.
[15] Haroun MA, Housner GW. Earthquake response of deformable liquid storage tanks. ASME Journal of Applied Mechanics 1981;48(2):411–8.
[16] Veletsos AS, Yang JY. Earthquake response of liquid storage tanks-advances in civil engineering through mechanics, In: Proceedings of the second ASCE engineering mechanics specialty conference. 1977. p. 1–24.
[17] Veletsos AS. Seismic response and design of liquid storage tanks. Guidelines for the seismic design of oil and gas pipeline systems. New York: ASCE Technical Council on Lifeline Earthquake Engineering; 1984. p. 255–370, 443–61.
[18] Malhotra P, Veletsos AS. Uplifting response of unanchored liquid storage tanks. ASCE Journal of Structural Engineering 1994;120(12):3525–47.
[19] American Petroleum Institute. API Standard 650. Steel tanks for oil storage, 8th ed. Washington (DC); 1988.
[20] ABAQUS Explicit User Manual, version 6.4. Hibbit, Karlsson and Sorensen; 2002.
[21] ABAQUS Theory Manual, version 6.4. Pawtucket (RI, USA): Hibbit, Karlsson and Sorensen; 2002.
[22] Veletsos AS, Shivakumar P. Tanks containing liquids or solids. Beskos DE, Anagnostopoulos SA, editors. Computer analysis and design of earthquake resistant structures: A handbook, vol. 3. Southampton (UK): Computational Mechanics Publications; 1997. p. 725–73.
[23] Virella JC, Suárez LE, Godoy LA. Effect of pre-stress states on the impulsive modes of vibration of cylindrical tank–liquid systems under horizontal motions. Journal of Vibration and Control 2005;11(9): 1195–220.
[24] Virella JC, Godoy LA, Suárez LE. Fundamental modes of tank–liquid systems under horizontal motions. Engineering Structures 2005 [in press].
[25] Uniform Building Code. Structural engineering design provisions, vol. 2. Whittier (CA): International Conference of Building Officials; 1997.
[26] Choun YS, Yun CB. Sloshing analysis of rectangular tanks with a submerged structure by using small-amplitude water wave theory. Earthquake Engineering and Structural Dynamics 1999;28:763–83.
[27] Budiansky B, Roth S. Axisymmetric dynamic buckling of clamped shallow spherical shells. NASA collected papers on stability of shell structures, TN-1510. 1962. p. 597–606.
[28] Babcock CD, Baker WE, Fly J, Bennet JG. Buckling of steel containment shells under time-dependent loading. In: Mechanical/structural engineering branch division of engineering technology. Washington (DC): Office of Nuclear Regulatory Commission; 1984.
[29] Tanami T, Taki S, Hangai Y. Dynamic buckling of shallow shells under the up-and-down earthquake excitation. In: Proceedings of the ninth world conference on earthquake engineering, vol. V. 1988. p. 545–50.
[30] Auli W, Rammerstorfer FG. On the dynamic instability of shell structures — criteria and algorithms. In: Finite element methods for plate and shell structures. Formulations and algorithms, vol. 2. Swansea (UK): Pineridge Press; 1986. p. 48–52 [Chapter 3].
[31] Hjelmstad KD, Williamson EB. Dynamic stability of structural systems subjected to base excitation. Engineering Structures 1988;20(4–6): 425–32.
[32] Godoy LA. Theory of elastic stability: Analysis and sensibility. Philadelphia (PA): Taylor and Francis; 2000.